JOURNAL OF GUIDANCE, CONTROL, AND DYNAMICS
Vol. 18, No. 2, March–April 1995

# Modeling and Control for Vibration Suppression of a Flexible Active Structure

Jeffrey Dosch*
*AVC Instrumentation, Depew, New York 14227*
Donald Leo†
*State University of New York at Buffalo, Buffalo, New York 14260*
and
Daniel Inman‡
*Virginia Polytechnic Institute and State University, Blacksburg, Virginia 24061*

**Theoretical and experimental results of the modeling and control of a flexible ribbed antenna are presented. The antenna consists of eight flexible ribs that constitute an active antenna in the sense that the actuators and sensors are an integral part of the structure. The antenna exhibits closely spaced and repeated modes, thus multi-input, multi-output (MIMO) control is necessary for controllability and observability of the structure. The structure also exhibits a mode localization phenomenon and contains postbuckled members making an accurate finite element model of the structure difficult to obtain. An identified MIMO minimum-order model of the antenna is synthesized from identified single-input, single-output transfer functions curve fit in the frequency domain. The identified model is used to design a positive position feedback and $H_\infty$ controller that increases damping in all of the modes in the targeted frequency range. Because of the accuracy of the open-loop model of the antenna, the closed-loop response predicted by the identified model correlates well with experimental results.**

## I. Introduction

AN accurate model of an active structure is fundamental to the understanding of control structure interaction. An active, or smart, structure contains a number of integrated sensors and actuators that allow the structure to perform precision pointing, sighting, placement, or vibration suppression to a degree of accuracy or performance not easily achieved with a passive structure. In the initial stages of design a finite element model (FEM) is adequate. The FEM allows one to address such issues as optimal actuator and sensor placement, size and power requirements of the actuators, and open- and closed-loop performance comparisons. Typically the FEM will accurately predict the natural frequencies of the structure and give a general idea of the mode shape of the structure, at least at low frequencies. The FEM will less accurately predict input/output transfer function parameters such as the zeros and the phase-vs-frequency response. In addition, standard FEM methods make no predictions of the damping in the system.

A structure such as the ribbed antenna addressed here presents two additional difficulties in obtaining an accurate FEM: mode localization and postbuckled beams. The periodic structure of the antenna results in the mode localization phenomenon where small perturbations in the manufacturing tolerance of parts of the structure can lead to large changes in the dynamics of the antenna.[1] The buckled ribs, which are a result of the antenna construction, make it difficult to use standard finite elements (such as beam or plate elements). In the construction of the antenna the ribs are initially flat and buckled into a dish shape by tension in the wire connected at the tip of each rib.

Because of the difficulties in obtaining an accurate FEM, an experimentally identified model is typically used for controller design. Most multi-input, multi-output (MIMO) identification techniques, such as the eigensystem realization algorithm (ERA), are batch techniques in which a MIMO model is obtained directly from test data after a model order is identified based on singular-value decomposition.[2] Previous work by Garcia et al.[3] used the ERA technique to identify a flexible antenna structure. In this paper a nonbatch, two-step identification technique is used. In the first step single-input, single-output (SISO) pole-zero transfer functions are curve fit in the frequency domain. In the second step the SISO transfer functions are synthesized into a MIMO model. An advantage of this method is that in the first step of the process each identified SISO transfer function can be adjusted if necessary to best correlate with the experimental response. It is much easier to adjust the SISO model to correlate with experimental response data than it is to adjust an MIMO model to match the experimental response. After the user is assured that each of the SISO transfer functions is correct, the SISO transfer functions are synthesized into an MIMO model.

The paper is organized as follows. In Sec. II, the active antenna construction and open-loop dynamic characteristics are described. In Sec. III a model identification technique in which the SISO transfer functions are synthesized into an MIMO model is presented and the method applied to identification of the active antenna. In Sec. IV the identified model is used to find the best actuator and sensor locations for maximum controllability and observability. Section V describes the design and experimental implementation of a positive position feedback (PPF) controller and an $H_\infty$ robust compensator for vibration suppression in the active antenna.

## II. Experimental Structure

Modern satellites often contain ribbed antennae or other flexible appendages. The vibrations of such flexible structures can often reduce the overall performance of the satellite. The active antenna described in this paper serves as a testbed for the vibration suppression of such structures using active control. With the exception of the inclusion of piezoelectric elements, the test antenna is similar (but smaller in scale) to the passive antenna, which is part of the Control Structure Interaction (CSI) Evolutionary Model located at NASA Langley.[4] Located at the base of five of the test antenna ribs are collocated piezoceramic sensor-actuator pairs. Each collocated sensor-actuator is manufactured from a single sheet of piezoelectric material of dimension $0.0152 \times 6.4 \times 2.3$ cm. The electrode surface of the piezoceramic is separated into two electrically isolated areas (Fig. 1). The sensor portion of the piezoceramic is connected to a

Received Oct. 6, 1993; revision received May 13, 1994; accepted for publication May 18, 1994. 

*Senior Engineer.
†Research Assistant.
‡Samuel Herrick Professor.

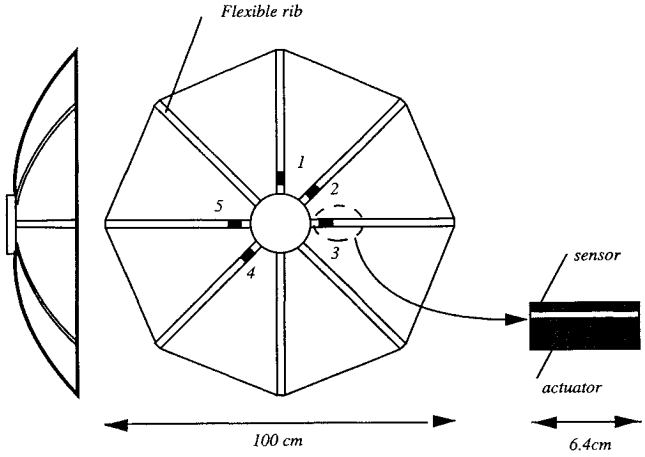


**Fig. 1 Schematic of active antenna.**

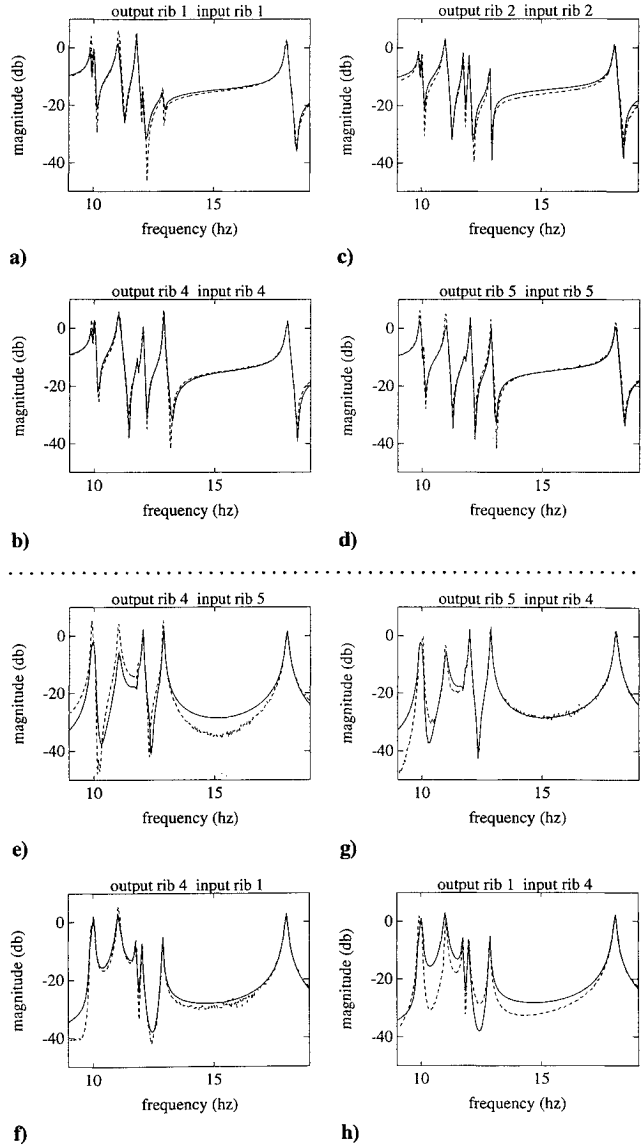


**Fig. 2 Magnitude plots of active antenna: a–d) collocated and e–h) noncollocated. Solid line, model; dashed line, experimental data.**

high-input impedance-measuring device and is a measure of strain in the rib.[5] Each rib is fixed at the base to a rigid hub and the tips are connected with tensioning wires. In the construction of the antenna, the ribs are initially flat and are brought to the dish shape by shortening of the tensioning wire.

A typical open-loop response for frequencies from 9 to 19 Hz is presented in Fig. 2. A cluster of seven closely spaced modes is observed between 9.6 and 17 Hz. A second cluster of modes can be observed near 30 Hz and subsequent clusters at subsequently higher frequencies. The first group of modes corresponds to each individual rib vibrating in its first mode, the second cluster corresponds to each rib vibrating in its second mode, etc. There are eight ribs, and it would be expected that eight modes exist in the first modal cluster. Only seven peaks can be observed; thus there is a repeated mode with a multiplicity of 2 in this first cluster, which can only be identified with a complete MIMO identification. The existence of a repeated mode with a multiplicity of 2 indicates that at least two actuators and two sensors are required for controllability and observability.

## III. Modeling Background

### MIMO Model Synthesis

Here a method for synthesizing a MIMO model from SISO transfer functions is described and is based on modal analysis techniques. With this method it is assumed that a pole-zero representation of the SISO transfer function is identified from either frequency-domain or time-domain data. A model based on modal analysis techniques offers two advantages over other modeling techniques. The modal model retains a simple physical correspondence between the identified model and the test structure, which is lost in many state-space identification methods. Another advantage is that by making symmetry assumptions about the structure (i.e., the mass, stiffness, and damping matrices are symmetric) the modal parameters can be obtained from a relatively small number of experimental transfer function measurements. The advantage of synthesizing the MIMO model from SISO representations is greater flexibility in matching the model to the experimental data.

The structure can be represented by

$$M\ddot{\hat{q}} + C\dot{\hat{q}} + K\hat{q} = u \tag{1}$$

where $M$, $C$, and $K$ are symmetric and positive definite matrices, $\hat{q}$ is a vector of displacements, and $u$ is a vector of inputs. It is also assumed that the structure is time invariant and a driving point transfer function (collocated sensor and actuator) is available. There are methods available for structures that do not conform to these assumptions: Ewins[7] discusses the problem of using modal identification on nonlinear systems and Inman[8] discusses modal identification for asymmetric $M$, $C$, and $K$ matrices.

Equation (1) can be cast in symmetric state-space form as

$$G\dot{q} - Hq = f \tag{2}$$

where

$$q = \begin{bmatrix} \hat{q} \\ \dot{\hat{q}} \end{bmatrix}, \qquad G = \left[\begin{array}{c|c} C & M \\ \hline M & 0 \end{array}\right],$$
$$H = \left[\begin{array}{c|c} -K & 0 \\ \hline 0 & M \end{array}\right], \qquad f = \begin{bmatrix} u \\ 0 \end{bmatrix} \tag{3}$$

There exists a transformation matrix $\Psi$ orthogonal with respect to $G$ that will diagonalize the system in Eq. (2):

$$\Psi^T G \Psi = I, \qquad \Psi^T H \Psi = \begin{bmatrix} \Lambda & 0 \\ 0 & \Lambda^* \end{bmatrix}$$
$$\Lambda = \operatorname{diag}(\lambda_r), \qquad \Lambda^* = \operatorname{diag}(\lambda_r^*) \tag{4}$$

The * symbolizes a complex conjugate. The transformation matrix $\Psi$ is partitioned in the following manner:

$$\Psi = \left[\begin{array}{c|c} \Phi & \Phi^* \\ \hline \Phi\Lambda & \Phi^*\Lambda^* \end{array}\right] \tag{5}$$

where the columns of $\Phi$ are the mode shape vectors of the system given in Eq. (1) and the rows of $\Phi$ are the modal participation vectors.

Substituting the transformation $q = \Psi x$ into Eq. (2) results in the diagonal equation

$$\dot{x} = \left[\begin{array}{c|c} \Lambda & 0 \\ \hline 0 & \Lambda^* \end{array}\right] x + \Psi^T f \tag{6}$$

Equation (6) can now be cast in the familiar state-space formulation

$$\dot{x} = Ax + Bu, \qquad y = C_0 x + Du \tag{7}$$

where

$$A = \left[\begin{array}{c|c} \Lambda & \mathbf{0} \\ \hline \mathbf{0} & \Lambda^* \end{array}\right], \qquad B = \left[\begin{array}{c} \Phi^T \\ \hline \Phi^{*T} \end{array}\right], \qquad C_0 = \left[\begin{array}{c|c} \Phi & \Phi^* \end{array}\right] \tag{8}$$

and $D$ is the direct transmission matrix. The objective of the modal modeling is to identify the $A$, $B$, $C_0$, and $D$ matrices in Eq. (8). The columns of $C_0$ (also the rows of $B$) are the mode shapes and are designated $c_r$ where $r$ can take values from 1 to $2n$ [$n$ is the number of degrees of freedom (DOF) retained in the model]. The columns of $B$ (and the rows of $C_0$) are the modal participation vectors and are designated $b_i$, where $i$ can take values from 1 to $m$ ($m$ is the number of measurement locations). Note that in the identified model the number of columns of $B$ is not necessarily equal to $2n$ but will instead depend on the number of experimental measurement locations. The $i$th element of the $r$th row of $\Phi$ is designated $\phi_{ir}$ and is called the modal participation factor. Taking the Laplace transform of Eq. (7) and substituting Eq. (8) result in an input/output relationship involving the receptance matrix $\alpha$:

$$\boldsymbol{Y}(s) = C_0(sI - A)^{-1}B\boldsymbol{U}(s) + D\boldsymbol{U}(s) \tag{9}$$

$$\boldsymbol{Y}(s) = \alpha(s)\boldsymbol{U}(s) \tag{10}$$

where

$$\alpha(s) = \left[\begin{array}{c|c} \Phi & \Phi^T \end{array}\right] \left[\begin{array}{c|c} (sI - \Lambda)^{-1} & \mathbf{0} \\ \hline \mathbf{0} & (sI - \Lambda^*)^{-1} \end{array}\right] \left[\begin{array}{c} \Phi \\ \hline \Phi^T \end{array}\right] + D \tag{11}$$

**Distinct Eigenvalue Case**

It follows from Eq. (10) that the transfer function between the $i$th output and the $j$th input is

$$\frac{Y_i(s)}{U_j(s)} = \sum_{r=1}^{n} \frac{\phi_{ir}\phi_{jr}}{s + \lambda_r} + \sum_{1}^{n} \frac{\phi_{ir}^*\phi_{jr}^*}{s + \lambda_r^*} + d_{ij} \tag{12}$$

where $d_{ij}$ is the $ij$ element of the matrix $D$ and the subscripts on $\phi$ indicate the corresponding element of the modal participation matrix. The asterisk denotes a complex conjugate. In general the numerators of Eq. (12) may have both real and imaginary parts, and in the normal-mode assumption (proportional or modal damping) the numerators will be purely imaginary. The experimental transfer function between the $i$th output and $j$th input is measured to be

$$\frac{\hat{Y}_i(s)}{\hat{U}_j(s)} = \sum_{r=1}^{n} \frac{{}_r\hat{A}_{ij}}{s + \hat{\lambda}_r} + \sum_{r=1}^{n} \frac{{}_r\hat{A}_{ij}^*}{s + \hat{\lambda}_r^*} + \hat{d}_{ij} \tag{13}$$

The "hat" notation denotes an experimentally measured quantity and ${}_r\hat{A}_{ij}$ is the residue between the $i$th output and the $j$th input for the $r$th eigenvalue. The modal participation factors $\phi_{ir}$ are identified by equating the numerator terms of Eq. (12) with the numerator terms of Eq. (13):

$$\phi_{ir}\phi_{\beta r} = {}_r\hat{A}_{i\beta}, \qquad i = 1, \ldots, m, \qquad r = 1, \ldots, n \tag{14}$$

which describes $m \times n$ equations and $m \times n$ unknowns where the input is at the point $j = \beta$. There is a closed-form solution to the equations described by Eq. (14). The equation involving the driving point $j = i = \beta$ is solved first and $\phi_{\beta r}$ is found. The modal participation factor $\phi_{\beta r}$ is then the "seed" for solving the remaining equations. Thus in the distinct-mode case all the modal participation terms can be solved for from a single input $\beta$. When more than a single reference is available, Eq. (14) is overdetermined and the modal participation factors $\phi_{ij}$ can be solved by recasting Eq. (14) as a minimization problem. A best fit solution can be found by minimizing the cost function $J$:

$$J = \sum_{r=1}^{n} \| f_r \| \tag{15}$$

where $\| \cdot \|$ is the Euclidean norm and $f_r$ is defined as

$$f_r = \phi_{ir}\phi_{\beta r} - {}_r\hat{A}_{i\beta} \tag{16}$$

**Repeated-Eigenvalue Case**

Here we show that when the eigenvalue is repeated with a multiplicity of 2 and the associated eigenvectors are linearly independent, a minimum of two inputs are required to identify the modal participation terms $\phi_{jr}$. This can be extended to show that when an eigenvalue is repeated with a multiplicity of $q$, a minimum of $q$ reference input locations are necessary to obtain a determined set of equations. Assume the first $p$ modes are repeated with a multiplicity of 2 and the remaining modes are distinct. The transfer function between input $j$ and output $i$ is then

$$\frac{Y_i(s)}{U_j(s)} = \sum_{r=1}^{p} \frac{{}_1\phi_{ir}\,{}_1\phi_{jr} + {}_2\phi_{ir}\,{}_2\phi_{jr}}{s + \lambda_r} + \sum_{r=1}^{p} \frac{{}_1\phi_{ir}^*\,{}_1\phi_{jr}^* + {}_2\phi_{ir}\,{}_2\phi_{jr}^*}{s + \lambda_r^*}$$
$$+ \sum_{r=p+1}^{n-2p} \frac{\phi_{ir}\phi_{jr}}{s + \lambda_r} + \sum_{r=p+1}^{n-2p} \frac{\phi_{ir}^*\phi_{jr}^*}{s + \lambda_r^*} + d_{ij} \tag{17}$$

The subscript preceding $\phi_{jr}$ (either a 1 or a 2) is used to differentiate between the two repeated modes associated with a repeated eigenvalue $r$. Equating the Eq. (17) numerator terms in with the identified transfer function Eq. (13) and using the input $j = \beta$ result in

$${}_1\phi_{ir}\,{}_1\phi_{\beta r} + {}_2\phi_{ir}\,{}_2\phi_{\beta r} = {}_rA_{i\beta}, \qquad i = 1, \ldots, m$$
$$r = 1, \ldots, p \tag{18}$$

which yields $2m \times p$ unknowns and $m \times p$ equations. An additional $p(m - 1)$ equations can be obtained by using a second input $j = \gamma$:

$${}_1\phi_{ir}\,{}_1\phi_{\gamma r} + {}_2\phi_{ir}\,{}_2\phi_{\gamma r} = {}_r\hat{A}_{i\gamma}, \qquad i = 1, \ldots, m$$
$$i \neq \beta$$
$$r = 1, \ldots, p \tag{19}$$

which together with Eq. (18) yield $2m \times p - p$ equations. When the eigenvalues are repeated, there are an infinite number of mode-shape solutions associated with the repeated eigenvalue, and each of these solutions is related to another solution by an orthogonal similarity transformation (see the Appendix for an example). Thus another $p$ equations are obtained by arbitrarily setting

$${}_1\phi_{\beta 1} = {}_1\phi_{\beta 2} = {}_1\phi_{\beta 3} = \cdots = {}_1\phi_{\beta p} = 0 \tag{20}$$

Equations (18–20) yield the $2m \times p$ equations necessary to solve for the elements $\phi_{jr}$ using experimental transfer functions. As in the non-repeated-mode case of Eq. (14), the overspecified case can be cast as a minimization problem.

Note that for a multiplicity of 2 it is necessary to use two inputs to obtain a determined set of equations. When frequency response data are available from more than two reference inputs, Eqs. (18) and (19) are overdetermined and can be recast as an optimization problem by minimizing the cost function $J$:

$$J = \sum_{r=1}^{p} = \| f_{r\beta} + f_{r\gamma} \| \tag{21}$$

where

$$f_{r\beta} = {}_1\phi_{ir}\,{}_1\phi_{\beta r} + {}_2\phi_{ir}\,{}_2\phi_{\beta r} - {}_r\hat{A}_{i\beta} \tag{22}$$

$$f_{r\beta} = {}_1\phi_{ir}\,{}_1\phi_{\gamma r} + {}_2\phi_{ir}\,{}_2\phi_{\gamma r} - {}_r\hat{A}_{i\gamma} \tag{23}$$

## IV. Identification of Active Antenna

Using the procedure outlined in the previous section, an MIMO model of the test antenna is obtained. The objective is to obtain a minimal-order MIMO model valid over the frequency range 0–20

**Table 1 Modal assurance criterion for pairs of inputs as measured from two different ribs**

| Frequency, Hz | Ribs 1, 2 | Ribs 1, 4 | Ribs 1, 5 | Ribs 2, 4 | Ribs 2, 5 | Ribs 4, 5 |
|---|---|---|---|---|---|---|
| 9.90 | 0.98 | 0.93 | 0.97 | 0.92 | 0.96 | 0.98 |
| 10.03 | 0.89 | 0.96 | 0.87 | 0.86 | 0.75 | 0.86 |
| 11.01 | 0.67 | 0.21 | 0.01 | 0.39 | 0.37 | 0.22 |
| 11.77 | 0.99 | 0.98 | 0.88 | 0.96 | 0.89 | 0.89 |
| 12.01 | 0.96 | 0.96 | 0.98 | 0.93 | 0.95 | 0.99 |
| 12.88 | 0.99 | 0.99 | 0.95 | 0.99 | 0.93 | 0.96 |
| 18.04 | 0.99 | 0.99 | 0.99 | 0.99 | 0.99 | 0.99 |

Hz, which includes the first cluster of modes. The minimal-order model is controllable and observable and accurately reflects both the open- and closed-loop response of the structure over the frequency of interest. The identification involves the following steps.

1) SISO random vibration data are obtained between a number of ribs. The following permutations of output/input data are obtained from four of the active ribs: rib 1/rib 1, rib 2/rib 1, rib 4/rib 1, rib 2/rib 2, rib 4/rib 2, rib 5/rib 2, rib 4/rib 4, rib 5/rib 4, rib 5/rib 5 (rib numbers refer to Fig. 1).

2) The random response data are curve fit in the frequency domain to identify SISO pole-zero models.

3) The repeated mode is identified by calculating the modal assurance criterion (MAC) for a mode, as calculated for different pairs of inputs.[7] The MAC measures the orthogonality of two modes. If the calculated MAC for a mode as measured from two inputs results in a number close to 1, then the mode is probably not repeated. If the MAC results in a number much less than 1 for the pair of inputs, then the mode probably is repeated. The MAC, which is a measure of orthogonality, calculated for all combinations of the tested input pairs is given in Table 1. The low MAC numbers associated with the mode at 11.01 Hz indicate that there is a repeated eigenvalue at that frequency.

4) The modal participation factors $\phi_{jr}$ are calculated by minimizing Eq. (15) for the distinct-mode case and minimizing Eq. (21) for the repeated-mode case.

5) The model is cast in the modal state-space form of Eqs. (7) and (8). The diagonal $A$ matrix is composed of the system eigenvalues obtained from the poles of the SISO pole-zero models; the repeated poles are identified as such in step 3. The $B$ and $C$ matrices are constructed from the modal participation factors $\phi_{jr}$. The $D$ matrix is constructed from the SISO pole-zero models.

Open-loop comparison of the identified model with experimental data is shown in Figs. 2a–2h. The identification technique models the collocated transfer functions with minimal error, as shown by the magnitude plots in Figs. 2a–2d. Although not shown, the phase response of the collocated transfer functions has the same accuracy. In the case of the noncollocated sensors and actuators (Figs. 2e–2h), the experimental results are in good agreement with the identified model, but they are not as accurate as the collocated transfer functions. This is attributed to the asymmetry that exists in the structure. In the modeling procedure, it is assumed that a transfer function between input $j$ and output $i$ is identical to the corresponding transfer function between input $i$ and output $j$. In reality, this is not the case since the sensors and actuators on each rib are slightly offset from one another (see Fig. 1). The error that is introduced is illustrated in Figs. 2e, f. The experimental transfer function with input at rib 5 and output at rib 4 is similar, but not identical, to the transfer function with input at rib 4 and output at rib 5. Consequently, one of the identified transfer functions (Fig. 2e) contains more error than the other (Fig. 2f), since the model cannot reflect the asymmetry that exists between the noncollocated sensors and actuators. The same phenomenon is illustrated between ribs 1 and 4 (Figs. 2g, h).

## V. Controller Design and Implementation

Using the model identified in the previous section, a pair of active ribs that exhibit a high degree of controllability are identified and two separate MIMO closed-loop control laws are designed: positive position feedback (PPF) and a robust controller design using $H_\infty$ optimal control theory. Unlike the $H_\infty$ design, the PPF design is a decentralized controller (i.e., each sensor signal is fed back only to its associated collocated actuator) and utilizes second-order filters in the feedback path.

**Table 2 Controllability measures for pairs of ribs on active antenna**

| Mode Frequency, Hz | Ribs 1, 2 | Ribs 1, 4 | Ribs 1, 5 | Ribs 2, 4 | Ribs 2, 5 |
|---|---|---|---|---|---|
| 18.0480 | 0.9101 | 0.9419 | 0.9067 | 0.9071 | 0.8705 |
| 12.8800 | 0.3089 | 0.5455 | 0.4188 | 0.5919 | 0.4777 |
| 12.0143 | 0.3662 | 0.4319 | 0.5034 | 0.5244 | 0.5848 |
| 11.7736 | 0.6661 | 0.5806 | 0.5770 | 0.3822 | 0.3766 |
| 10.0326 | 0.5493 | 0.6626 | 0.4829 | 0.6043 | 0.3991 |
| 9.9087 | 0.5372 | 0.5122 | 0.6944 | 0.4909 | 0.6788 |
| 11.0103[a] | 0.3678 | 0.1654 | 0.4379 | 0.3202 | 0.2640 |

[a]Repeated mode.

### PPF Control

The PPF controller can be described by the second-order form

$$I\ddot{\boldsymbol{q}}_c + \Lambda_{Dc}\dot{\boldsymbol{q}}_c + \Lambda_{Kc}\boldsymbol{q}_c = \boldsymbol{u}_c \tag{24}$$

$$\boldsymbol{y}_{dc} = H_{dc}\boldsymbol{q}_c \tag{25}$$

$$\boldsymbol{u}_c = B_{dc}\boldsymbol{y}_d \tag{26}$$

where

$\Lambda_{Dc}(r \times r)$ = controller damping matrix diag$(2\zeta_{ci}\omega_{ci})$
$\Lambda_{Kc}(r \times r)$ = controller stiffness matrix diag$(\omega_{ci}^2)$
$\boldsymbol{q}_c(r \times 1)$ = controller coordinate
$H_{dc}(m \times r)$ = controller output gain matrix
$H_d(s_d \times n)$ = structure output gain matrix
$\boldsymbol{y}_d(s_d \times 1)$ = structure output
$\boldsymbol{y}_{dc}(r \times 1)$ = controller output
$\boldsymbol{u}_c(r \times 1)$ = controller input vector
$\boldsymbol{u}(m \times 1)$ = system input vector

where $n$ is structure degrees of freedom, $m$ is number of actuators, $r$ is number of control filters, and $s_d$ is number of displacement sensors.

The input to the active structure is coupled to the controller by

$$\boldsymbol{u} = (\boldsymbol{y}_{dc} - G_d\boldsymbol{y}_d) \tag{27}$$

where $B_{dc}$ is the controller input gain matrix and $G_d$ is a direct transmission matrix. The controller described by Eqs. (24–27) is called an active vibration absorber (AVA) by Juang and Phan.[9] The PPF control is derived from the AVA controller by setting the direct transmission term in Eq. (27) to zero:

$$\boldsymbol{u} = \boldsymbol{y}_{dc} \tag{28}$$

Advantages in using PPF control are the low-order and simple stability criterion. The PPF controller is stable as long as a simple inequality constraint is satisfied that involves the controller gains and the structural stiffness matrix.[10,11]

### Controllability Measures for Active Antenna

The definition of controllability provides only a yes-or-no answer to whether a system is controllable. On the other hand, a controllability measure will provide an answer to the degree of controllability of a mode. From a strict definition of controllability, it is known that a minimum of two active ribs are required on the experimental antenna to control the repeated mode at 11.01 Hz.[6] A controllability measure is used to determine which two of the four active ribs included in the identified model will provide a high degree of controllability.

Calculated from the identified model, Table 2 provides controllability measures for pairs of ribs. The table is based on the method of Hamden and Nayfeh[12] for the distinct modes and the method of Hughes and Skelton[6] for the repeated mode. The controllability measures with active ribs 1 and 5 are consistently high, and for this reason this pair is used in the experimental implementation of the MIMO control with two active ribs. A poor choice would be ribs 1 and 4, which show comparatively low controllability of the repeated mode at 11.0103 Hz.

**PPF Controller Implementation**

The PPF control laws are implemented on the active antenna and the closed-loop response compared with the response predicted by the model. The control laws are implemented digitally with a sampling rate of 1000 Hz. The AVA and PPF control were implemented on an earlier version of the active antenna in an SISO control environment.[11] The AVA controller with displacement feedback does not roll off, and thus the desired gain is limited by high-frequency dynamics, which are often unmodeled. The PPF was not affected by unmodeled high frequency dynamics resulting in better experimental performance. In fact it can be shown that as the gain is increased with the PPF controller the instability will result at low frequency, which is typically well modeled.[10]

A constrained optimization routine is used to design the PPF controller parameters $H_d$, $\Lambda_{Kc}$, and $\Lambda_{Dc}$. The optimization minimizes the cost function

$$J = \int_0^{t_f} (|y(t)| + w|u(t)|)\, dt \tag{29}$$

where $y(t)$ is the identified antenna model response to a unit impulse and $u(t)$ is the control effort. Values for the weight $w$ are adjusted to achieve the best trade-off between minimizing the impulse response and minimizing the control effort. The control is optimized for the closed-loop control operating on ribs 1 and 5.

In the control design each actuator is capable of having multiple filters associated with it, i.e., in the matrices $\Lambda_{Kc}(r \times r)$ and $\Lambda_{Dc}(r \times r)$, $r$ is not necessarily 1. It is found that no significant reduction in the cost function is obtained using multiple filters. This can be attributed to the fact that the modes are closely spaced and the model does not include higher frequency modes. Therefore, only a single filter per actuator is used in the implemented design. With a weight $w$ of 1, the optimal filter parameters are found to be $\omega_c = 70.2$ rad/s and $\zeta_c = 0.56$.

The experimental response of the antenna with PPF control on ribs 1 and 5 is compared with the predicted response and also with the open-loop response (Figs. 3a and 3b). Significant damping is achieved in all the modes in the first modal cluster using only a single PPF filter on each of the two active ribs.

**$H_\infty$ Controller Implementation**

A robust controller designed using $H_\infty$ optimal control theory is also implemented on the active antenna. In comparison to the collocated controllers discussed previously, $H_\infty$ theory explicitly deals with the multivariable control problem as well as accounting for the uncertainty that exists in the nominal model.[13,14]

The robust control design is begun by augmenting the nominal model by the performance and uncertainty weights (Fig. 4). The uncertainty in the system is modeled as multiplicative at the output to account for the errors in the identified transfer functions. Although the model agrees well with the experimental results, errors do exist, especially in the noncollocated sensor/actuator pairs. Performance is measured by the vibration suppression achieved to a remote disturbance on the antenna. This is accomplished in the $H_\infty$ design by increasing the value of $\gamma$, thereby forcing the controller to suppress the flexible modes in the frequency range of interest. For the active antenna, the robust controller targets the group of eight modes below 20 Hz.

The choice of performance and uncertainty weights determines the closed-loop response of the structure. The multiplicative uncertainty weights $W_1$ and $W_2$ are chosen as a first-order lead filter, with a break frequency of approximately 100 rad/s. The gain of the filter specifies that, at low frequencies, the assumed error in the model is 25% and increases at higher frequencies due to the unmodeled dynamics. The performance weights $W_5$ and $W_6$ for the vibration suppression are a first-order lag filter that rolls off after 100 rad/s. This specifies that vibration suppression is desired for only the low-frequency dynamics ($\lesssim$20 Hz). The final set of weights ($W_3$ and $W_4$) determines the shape of the controller. Since it is important for the controller to roll off at higher frequencies, the weight increases sharply throughout the region of interest (similar to a differentiator). High-frequency roll-off of the controller is necessary so that

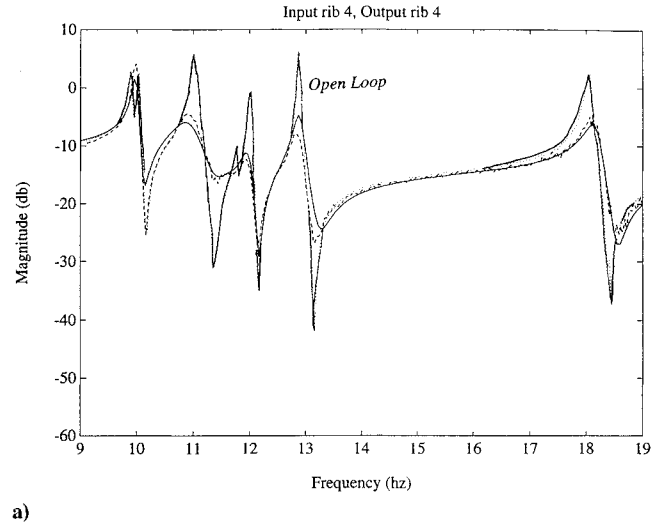


a)

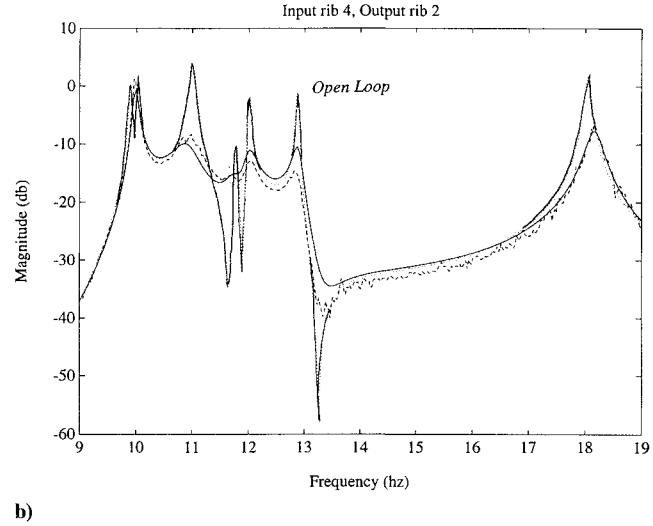


b)

**Fig. 3 Comparison between open-loop transfer functions (labeled solid line), closed-loop experimental (dashed line), and predicted closed-loop response (unlabeled solid line).**

unmodeled dynamics are not destabilized by the active control. Finally, a small weight is added to the augmented plant to account for the noise present in the sensor signal:

$$W_{1,2}(s) = \frac{0.25(s/100 + 1)}{s/1250 + 1}$$

$$W_{3,4}(s) = \frac{0.1(s + 1)}{s/1000 + 1} \tag{30}$$

$$W_{5,6}(s) = \frac{0.2(s/1000 + 1)}{s/100 + 1}$$

With this choice of weights, a robust controller is designed by the $\gamma$-iteration technique. The scalar gain $\gamma$ is increased until either the maximum robust performance or robust stability bound equals 1, indicating that a further increase in $\gamma$ would cause one of the robustness criteria to be violated. The block structure of the uncertainty is chosen to be one 2 × 2 block and a second 3 × 4 block, to account for the coupling in the performance and stability measures. In all designs, the robust performance bound determined the maximum value of $\gamma$. The order of the controller is reduced from 22 states to 19 states using a Schur balanced model reduction technique.

Implementation of the $H_\infty$ compensator on the active antenna increased the damping in the structure in the region of the first modal cluster (Fig. 5). The increase in damping is not as significant as

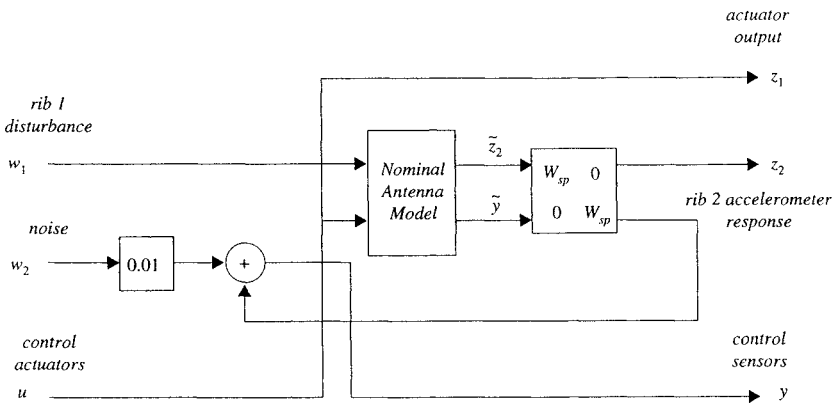


**Fig. 4 Augmented plant for robust control design.**

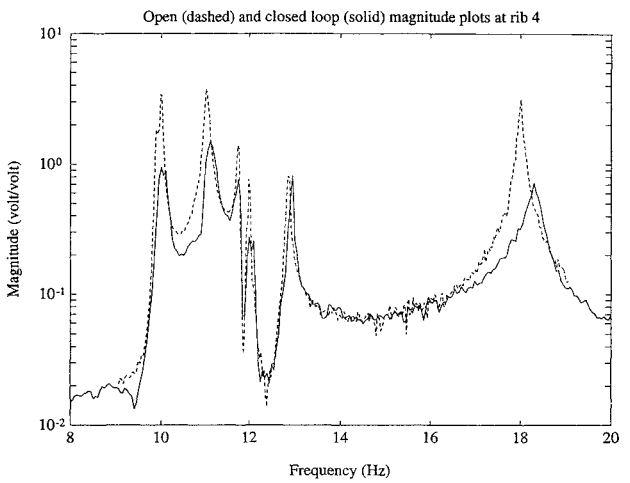


**Fig. 5 Magnitude plot with $H_\infty$ control loop closed.**

with the PPF controller due to the difficulty in the design of the MIMO compensator. The limiting factor for the active antenna is the trade-off of performance in the low-frequency region (0–20 Hz) vs stability of the unmodeled modes lying between 30 and 40 Hz. To assure stability, it is necessary to have a sharp roll-off of the controller, thus reducing the amount of vibration suppression achieved in the closed loop. During the design, it is apparent that reducing the roll-off of the controller improves the closed-loop damping but results in an unstable system when implemented on the actual structure. The final set of weights obtained the best performance without destabilizing the unmodeled dynamics.

## VI. Conclusions

A study in the control of an eight-ribbed active antenna was performed that investigated issues in modeling, actuator location for controllability, control design, and control implementation. The active antenna is an ideal structure for such an investigation for a number of reasons: It is difficult to obtain a FEM of such a structure; the repeated modes necessitates an MIMO control architecture; the lightweight, delicate nature of the antenna ribs excludes the use of bulky actuators; and control of such structures has important applications in space satellites.

A minimal-order model of the antenna was identified by synthesizing a MIMO model from SISO transfer functions. Synthesizing the model from the SISO transfer functions gives the modeling user greater flexibility in matching the model to the experimental data. Using this identification method on the active antenna, good correlation between the predicted response and the open-loop antenna response was obtained. The model also gave a good prediction of the closed loop behavior, which is important for closed-loop control design. This can be contrasted with many identification techniques that overestimate the model order size, resulting in a non-minimal-order model. Such a model may produce good open-loop correlation with experimental data but give inaccurate closed-loop predictions. This is because with a non-minimal-order model there are dynamics in the model that are not in the actual structure.

Closed-loop control was implemented on the antenna using PPF and $H_\infty$ control laws. For the PPF design, the identified model was used to optimize the controllers. Using a single PPF filter on two of the active antenna ribs, the first cluster of eight modes was actively damped. The robust controller design did not increase the damping as significantly as the collocated position compensators. This was due to the difficult trade-off between suppressing the flexible modes and maintaining stability of the unmodeled dynamics. Also, the block-diagonal structure of the PPF controllers (no coupling between noncollocated sensors and actuators) produced a compensator that exploited the benefits of the sensor-actuator collocation.

## Appendix

Using a simple example, here it is shown that for a repeated eigenvalue one of the modal participation terms in one of the repeated modes can be arbitrarily set to zero. It is important to keep in mind that when the eigenvalues are distinct the rows of the $B$ matrix (the mode shapes) are uniquely determined from experimental data. When the eigenvalues are repeated, there are an infinite number of mode-shape solutions associated with the repeated eigenvalue, and each of these solutions is related to another solution by an orthogonal similarity transformation. Thus for the system given by Eqs. (7) and (8) there exists an orthogonal similarity transformation $T$ such that

$$x = T^T q, \qquad T^T A T = A, \qquad \tilde{B} = T^T B \tag{A1}$$

Note that the $A$ matrix (the matrix of eigenvalues) is unaffected by the transformation, whereas certain rows of the $B$ matrix are transformed and other rows are unaffected. Those rows of $B$ that are associated with distinct eigenvalues are unaffected by the transformation $T$ and those rows associated with repeated eigenvalues may be transformed. This result is best shown by a simple example. Given is the following system with distinct eigenvalues $a$ and $c$ and repeated eigenvalue $b$:

$$\dot{x} = Ax + Bu$$

$$A = \begin{bmatrix} a & & & \\ & b & & \\ & & b & \\ & & & c \end{bmatrix}, \qquad B = \begin{bmatrix} d_1 & d_2 & d_3 & d_4 \\ e_1 & e_2 & e_3 & e_4 \\ f_1 & f_2 & f_3 & f_4 \\ g_1 & g_2 & g_3 & g_4 \end{bmatrix} \tag{A2}$$

An orthogonal similarity transformation is arbitrarily chosen to be

$$T = \begin{bmatrix} 1 & 0 & 0 & 0 \\ 0 & \cos\theta & -\sin\theta & 0 \\ 0 & \sin\theta & \cos\theta & 0 \\ 0 & 0 & 0 & 1 \end{bmatrix} \tag{A3}$$

Applying the transformation $x = T^T q$ to Eq. (A2), it is found that $T^T T = I$, $T^T A T = A$, and

$$\tilde{B} = T^T B = \begin{bmatrix} d_1 & d_2 & d_3 & d_4 \\ e_1 \cos\theta - f_1 \sin\theta & e_2 \cos\theta - f_2 \sin\theta & e_3 \cos\theta - f_3 \sin\theta & e_4 \cos\theta - f_4 \sin\theta \\ e_1 \cos\theta + f_1 \sin\theta & e_2 \cos\theta + f_2 \sin\theta & e_3 \cos\theta + f_3 \sin\theta & e_4 \cos\theta + f_4 \sin\theta \\ g_1 & g_2 & g_3 & g_4 \end{bmatrix} \tag{A4}$$

Note that the first and fourth rows of $\tilde{B}$ are the same as the first and fourth rows of $B$. These are the row associated with the distinct modes. Note also that any single element of the repeated mode shapes can be arbitrarily set to zero by judicious choice of the transformation $T$. For instance the element in the second row, first column of $\tilde{B}$ will be equal to zero if $\theta$ is chosen such that $\theta = \tan^{-1}(e_1/f_1)$.

## Acknowledgments

This work was supported by Air Force Office of Scientific Research Grant 91-0181 (JD), NASA Grant NAG 1 1462 (DJL), and ARO Grant DAAL0391G0063 (DJI).

## References

[1]Levine-West, M. B., and Salama, M. A., "Mode Localization Experiments on a Ribbed Antenna," *Proceedings of the 33rd AIAA/ASME/ASCE/AHS/ASC Structures, Structural Dynamics, and Materials Conference* (Dallas, TX) AIAA, Washington, DC, 1992, pp. 2038–2047.

[2]Juang, J.-N., and Pappa, R. S., "An Eigensystem Realization Algorithm for Modal Parameter Identification and Model Reduction," *Journal of Guidance, Control, and Dynamics*, Vol. 8, No. 5, 1985, pp. 620–627.

[3]Garcia, E., Dosch, J., and Inman, D. J., "The Application of Smart Structures to the Vibration Suppression Problem," *Journal of Intelligent Material Systems and Structures*, Vol. 3, No. 4, 1992, pp. 659–667.

[4]Belvin, W. K., Horta, L. G., and Elliot, K. B., "The LaRC CSI Phase-0 Evolutionary Model Test Bed—Design and Experimental Results," *Proceedings of the 4th Annual NASA/DoD Conference on Control/Structure Interaction* (Orlando, FL), Nov. 1990.

[5]Dosch, J. J., Inman, D. J., and Garcia, E., "A Self-Sensing Piezoelectric Actuator for Collocated Control," *Journal of Intelligent Materials and Structures*, Vol. 3, No. 1, 1992, pp. 166–185.

[6]Hughes, P. C., and Skelton, R. E., "Controllability and Observability of Linear Matrix-Second-Order Systems," *ASME Journal of Applied Mechanics*, Vol. 47, 1980, pp. 415–420.

[7]Ewins, D. J., *Modal Testing: Theory and Practice*, Wiley, New York, 1986.

[8]Inman, D. J., "Modal Analysis for Asymmetric Systems," *Proceedings of the 1st International Modal Analysis Conference* (Orlando, FL), Jan. 1982, pp. 705–708.

[9]Juang, J.-N., and Phan, M., "Robust Controller Design for Second Order Dynamic Systems: A Virtual Passive Approach," *Proceedings of the 32nd AIAA/ASME/ASCE/AHS/ASC Structures Structural Dynamics, and Materials Conference* (Baltimore, MD), AIAA, Washington, DC, 1991, pp. 1796–1805.

[10]Fanson, J. L., and Caughey, T. K., "Positive Position Feedback Control for Large Space Structures," *Proceedings of the 28th AIAA/ASME/ASCE/AHS/ASC Proceedings 28th AIAA Structures Structural Dynamics, and Materials Conference* (Monterey, CA), AIAA, Washington, DC, 1987, pp. 588–598.

[11]Dosch, J. J., Leo, D. J., and Inman, D. J., "Comparison of Vibration Control Schemes for a Smart Antenna," *Proceedings of the 31st Conference on Decision, and Control* (Tucson, AZ), AIAA, Washington, DC, 1992, pp. 1815–1820.

[12]Hamdan, A. M. A., and Nayfeh, A. H., "Measures of Modal Controllability and Observability for First- and Second-Order Linear Systems," *Journal of Guidance, Control, and Dynamics*, Vol. 12, No. 3, 1989, pp. 421–428.

[13]Stein G., and Doyle, J. C., "Beyond Singular Values and Loop Shaping," *Journal of Guidance, Control, and Dynamics*, Vol. 14, No. 1, 1991, pp. 5–15.

[14]Moser, A. N., "Designing Controllers for Flexible Structures with $H_\infty$/$\mu$-Synthesis," *IEEE Control Systems Magazine*, April 1993, pp. 79–89.